Modulating the Electronic Metal-Support Interactions in Single-Atom Pt_1 CuO Catalyst for Boosting Acetone Oxidation

Zeyu Jiang[+], Mingjiao Tian[+], Meizan Jing[+], Shouning Chai, Yanfei Jian, Changwei Chen, Mark Douthwaite, Lirong Zheng, Mudi Ma, Weiyu Song, Jian Liu, Jiaguo Yu, and Chi He**

Abstract: The development of highly active single-atom catalysts (SACs) and identifying their intrinsic active sites in oxidizing industrial hazardous hydrocarbons are challenging prospects. Tuning the electronic metal-support interactions (EMSIs) is valid for modulating the catalytic performance of SACs. We propose that the modulation of the EMSIs in a Pt_1 CuO SAC significantly promotes the activity of the catalyst in acetone oxidation. The EMSIs promote charge redistribution through the unified Pt O Cu moieties, which modulates the *d*-band structure of atomic Pt sites, and strengthens the adsorption and activation of reactants. The positively charged Pt atoms are superior for activating acetone at low temperatures, and the stretched Cu O bonds facilitate the activation of lattice oxygen atoms to participate in subsequent oxidation. We believe that this work will guide researchers to engineer efficient SACs for application in hydrocarbon oxidation reactions.

Introduction

The emission of organic hydrocarbons from industry poses a significant hazard to human health and the environment.[1] The development of technologies to eliminate the emission of volatile organic compounds (VOCs) is one of the biggest challenges facing the chemical industry in the 21st century.[1b] Oxygenated VOCs (OVOCs) are concerning because of their high propensity to form ozone and their extensive discharge from chemical industries.[2] Acetone, containing C=O, C C, and C H bonds, is a typical OVOC, which is one of the major pollutants discharged by pharmaceutical and package-printing industries.[3] There-fore, developing a strategy for efficient removal of acetone is of great importance.[4] Catalytic oxidation is a promising method to decompose hydrocarbons, at the core of which is constructing efficient catalysts.[5] Pt-based catalysts have been identified as effective materials for hydrocarbon removal.[2,6] Considering the cost of the active component (Pt), the single-atom catalysts (SACs) with maximum utilization efficiency are very promising in such reactions because of the coordinatively unsaturated nature of the atomic sites, which favors the activation of organic hydrocarbons.[7] For example, the supported Pt atoms are exceptionally active for methanol oxidation at low temperatures.[8] Nevertheless, in-depth analysis of the intrinsic mechanisms of SACs is limited by inhomogeneous bonding methods and the complicated processes that occur during reactant transformation. Therefore, it is imperative to design and synthesize SACs with unified coordination bonds to attain a reliable understanding of why these materials are so effective.[9]

Many reports have proven that the tunable electronic structure and unoccupied *d* state of single atoms renders them amenable to interactions with oxide supports.[9a] This is perceived as critical for stabilizing atomic sites and modulat-

[*] Dr. Z. Jiang,[+] Dr. M. Tian,[+] Prof. S. Chai, Dr. Y. Jian, Dr. C. Chen, Dr. M. Ma, Prof. C. He
State Key Laboratory of Multiphase Flow in Power Engineering, Xi'an Jiaotong University
Xi'an 710049, Shaanxi (P. R. China) E-mail: chi_he@xjtu.edu.cn

Dr. Z. Jiang[+]
Department of Chemistry,
National University of Singapore
Singapore 117543 (Singapore)

Dr. M. Tian,[+] Prof. J. Yu
Laboratory of Solar Fuel, Faculty of Materials Science and Chemistry, China University of Geosciences
Wuhan 430074 (P. R. China) E-mail: yujiaguo93@cug.edu.cn

Dr. M. Jing,[+] Prof. W. Song, Prof. J. Liu
State Key Laboratory of Heavy Oil Processing,
China University of Petroleum
Beijing 102249 (P. R. China)

Prof. M. Douthwaite
Max Planck-Cardiff Centre on the Fundamentals of Heterogeneous Catalysis, School of Chemistry, Cardiff University Cardiff, CF10 3AT (UK)

Dr. L. Zheng
Institute of High Energy Physics,
Chinese Academy of Sciences
Beijing 100049 (P. R. China)

Prof. C. He
National Engineering Laboratory for VOCs Pollution Control Material & Technology, University of Chinese Academy of Sciences Beijing 101408 (P. R. China)

[+] These authors contributed equally to this work.

ing their properties in catalysts.[10] Numerous studies have focused on tuning the electronic metal-support interactions (EMSIs) in SACs to promote their catalytic efficiency and stability.[11] One such example, by Datye et al.,[12] demonstrated that the interactions between Pt atoms and CeO_2 supports could be tuned by thermal restructuring, which significantly influenced their catalytic activity for CO oxidation. In a separate study by Tang and co-workers,[7c] the electronic structure of a Ag-based SAC was manipulated. The authors revealed that the higher depletion of the *d* electronic state of Ag atoms resulted in strong EMSIs with improved reducibility, which facilitated its superb catalytic activity towards formaldehyde oxidation.[7c] A similar observation has also been reported in our previous work.[13] The thermally stable Pt_1/CeO_2 SACs with strong EMSIs were constructed through stabilization with oxygen vacancies. These SACs exhibited an excellent stability for methanol oxidation, even after calcination at 800 °C.[13]

A common method employed to strengthen EMSIs is to target the anchoring of single atoms onto vacancies or lattice fringes. This is a highly efficient method for inducing such interactions but is limited by the specific oxide supports and can result in undefined coordination structures.[9a] Therefore, it is pertinent to develop a universal method for enhancing and tuning EMSIs with unified bonding. The surface of transition metal hydroxides is abundantly populated with -OH species, which could provide suitable anchoring sites for coordination with metal atoms through M O(OH) interactions.[9a] Examples of EMSIs between Pt and Ni/Fe/ Cu/Co-based hydroxides have already been developed.[14]

It is known that the electron transfer between Pt species and copper/cuprous oxides can occur readily.[15] Based on this, and the fact that CuO materials possess well-established redox properties (Cu^+ /Cu^{2+}), Pt_1 CuO could be an interest-ing catalyst to study EMSIs, through the calcination of Pt $Cu(OH)_x$ precursors. In this situation, the Pt atoms are expected to be stabilized by surface hydroxyl groups over $Cu(OH)_x$, and the associated EMSIs can be easily modu-lated by tuning the unified Pt O bonds. Additionally, the rational design of highly active catalysts requires a compre-hensive understanding of the structure–activity relationships. Hence, it is of great significance to reveal the intrinsic active sites and establish a structure–activity relationship for EMSI-modulated SACs through persuasive operando exper-imental methods.

Herein, Pt atoms are anchored onto CuO supports via different bonding strategies, resulting in the formation of diverse EMSIs. Specifically, a Pt_1 CuO catalyst with unified Pt O Cu coordination bonds exhibits the strongest EMSIs compared to those of the generally supported Pt_1/CuO and bulk-doping Pt_1@CuO samples. The results powerfully demonstrate that the modulation of a Pt_1 CuO SAC with EMSIs significantly promotes the low-temperature activity of the catalyst, over which 800 ppm of acetone can be totally decomposed at 210 °C with a GHSV of 42000 h^{-1}. The EMSIs facilitate the charge redistribution through electron transfer from Pt atoms to CuO supports, which modulates the *d*-band structure of Pt atoms, and strengthens the adsorption and activation of reactants. Hence, the energy barrier is lowered and the rate-limiting step is facilitated. The general effect of EMSI modulation is not limited to acetone oxidation, which is the primary model substrate for this study.

Results and Discussion

Structure and Atomic Sites

Three different methods were employed for the synthesis of SACs used herein (Figure 1). Primarily, the microwave-synthesized $Cu(OH)_x$ was adopted as the precursor of the support to stabilize platinum bis(acetylacetonate) in obtaining the Pt_1 $(OH)_x$ Cu complex. The Pt_1 CuO catalyst was synthesized via a calcination process of the aforementioned complex to form the unified Pt O Cu bonds. Subsequently, Pt atoms were supported on CuO via mixed Pt O and Pt Cu bonds that were established via a general impregna-tion method, forming the Pt_1/CuO catalyst. The Pt_1@CuO sample was formed by doping the Pt species into the bulk of CuO through an in-situ-doping process.

The nanorod CuO support exposes a dominant (111) facet to disperse Pt atoms, which were identified by high-resolution transmission electron microscopy (HR-TEM) images and DFT calculations (Supporting Information, Figures S1–S4).[16] As listed in Table S1 (Supporting Infor-mation), the actual Pt contents of the catalysts was maintained around ca. 0.40 wt%, and the dispersion of Pt species ranged from 64.6% to 84.5%. The supported Pt species had a negligible effect on the pore structure of the CuO support (Figure S5, Table S2). The atomic Pt sites of the SACs were identified with aberration-corrected scanning transmission electron microscopy (ac-STEM) using Z-con-trast (Figure 2a; Figure S6), which clearly demonstrated that

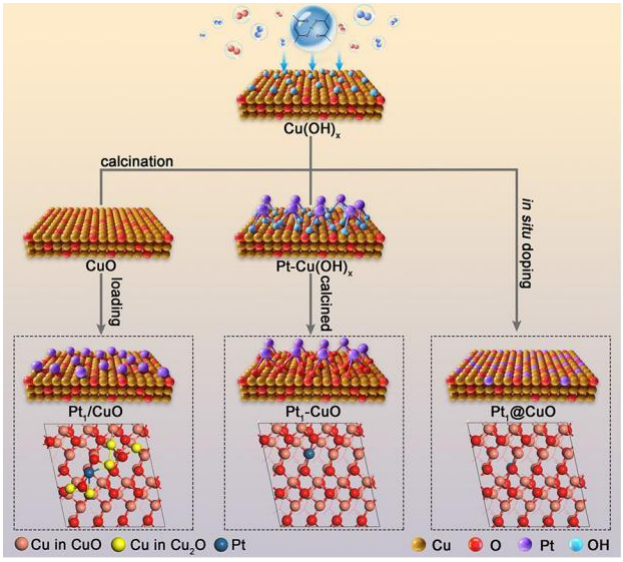

Figure 1. A description and optimized structure of the synthesized single-atom catalysts.

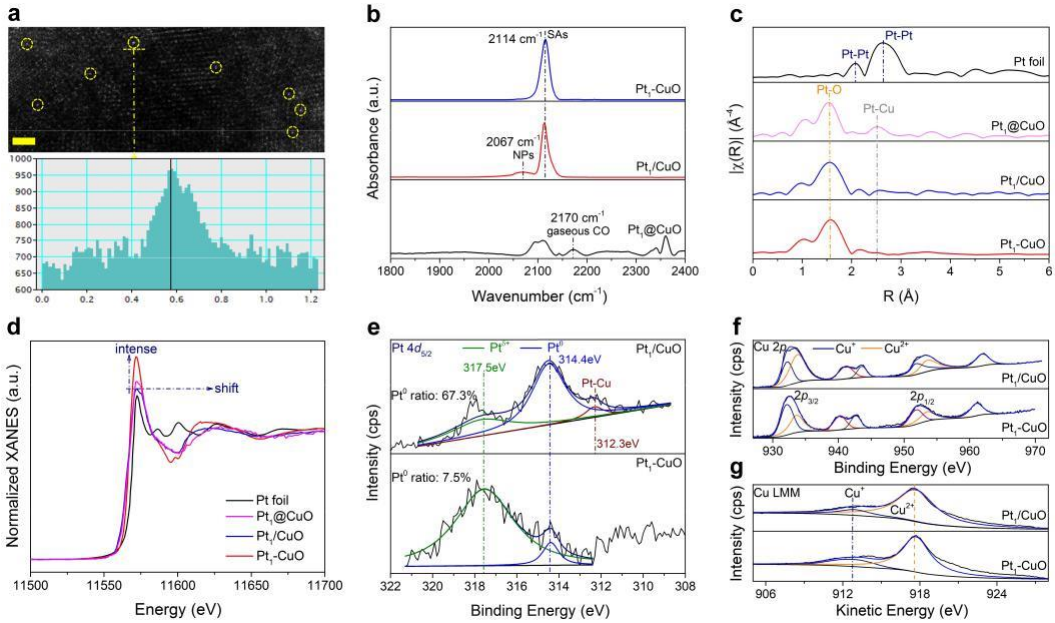

Figure 2. a) Aberration-corrected STEM image of single-atom Pt_1 CuO catalyst, scale bar: 1 nm. b) IR spectra of CO adsorption over synthesized catalysts. c) R-space spectra from Pt L_3-edge EXAFS data of prepared catalysts. d) Pt L_3-edge normalized XANES curves of prepared catalysts. e) Pt 4$d_{5/2}$, f) Cu 2p, and g) Cu LMM XPS spectra of prepared catalysts.

the isolated Pt atoms are present on the surface of the prepared catalysts.[17]

Each of the catalysts was subsequently investigated by infrared spectroscopy (IR), utilizing CO as a probe molecule (Figure 2b). In the spectra of Pt_1 CuO and Pt_1/CuO catalysts, sharp adsorption bands at ca. 2114 cm ^{1} are indicative of the CO Pt stretches, associated with the adsorption of CO on the cationic Pt atoms.[18] The band observed at ca. 2067 cm ^{1} for the Pt_1/CuO catalyst can be reasonably assigned to the linearly adsorbed CO molecules associated with the highly coordinated Pt nanoclusters, indicating that some tiny Pt clusters are also produced during the general impregnation process.[12] Notably, in the spectrum of the Pt_1@CuO catalyst a significant band at 2170 cm ^{1} is observed, which is indicative of the gaseous CO molecules on the CuO support.[19] The stronger gaseous CO adsorption band in this sample is attributed to the deficiently buried Pt sites that are doped in the CuO bulk.[20] Our DFT calculations predict top-adsorbed CO stretching frequencies of 2102, 2098, and 2070 cm ^{1} over Pt_1 CuO, Pt_1/ CuO, and Pt@CuO SACs, respectively, which are very close to experimentally observed locations (Figure S7, Table S3).[20b] Additionally, compared with the Pt_1 CuO catalyst, the calculated CO vibrational frequencies over Pt_1/ CuO and Pt@CuO SACs are slightly shifted to lower energies, which can be attributed to the higher coordinated Pt atoms from Pt Cu bonds and more Pt^0 species.[18b]

Subsequently, the detailed coordination structures were analyzed from the curve fitting of the Pt L_3-edge extended X-ray absorption fine structure (EXAFS), and the corresponding specific coordination environment information pertaining to the synthesized single-atom catalysts is displayed in Figure 2c and Figure S8. Prominent peaks centered at 1.56–1.58 and 2.53–2.55 Å are assigned to the Pt O and Pt Cu contributions, respectively. Referring to the Pt foil, almost no Pt Pt contribution can be observed over these single-atom catalysts. Subsequently, the coordination of Pt atoms with Pt O and Pt Cu bonding are included. The Pt_1 CuO catalyst exhibits a Pt O coordination number of 4.6 ± 0.05 with a radial distance of 1.58 ± 0.002 Å, and it possesses a Pt Cu coordination number of 0.7 ± 0.02 with a radial distance of 2.53 ± 0.002 Å (Table S4).[1,2] In compar-ison, the Pt Cu coordination number gradually increases for Pt_1/CuO (1.6 ± 0.01) and Pt_1@CuO (2.4 ± 0.04) catalysts, whereas the Pt O coordination number of these catalysts declines (from 4.0 ± 0.07 to 3.2 ± 0.02). The aforementioned coordination environments compare well to the DFT calculations (Figure S9).

Electronic Metal-Support Interactions

An in-depth analysis of the electronic structure on atomic sites is crucial for establishing structure–activity relationships.[11c] Therefore, several analyses were conducted to probe the EMSIs present in these SACs. Firstly, the Pt L_3-edge X-ray absorption near-edge structure (XANES) was examined (Figure 2d). In-depth analysis reveals that the absorption intensity of the synthesized Pt-based SACs is higher than that observed in the Pt foil, indicating that positively charged Pt species are present in these SACs.[17,21] The white line (WL) exhibited by the Pt_1 CuO sample is notably more intense than that observed over the Pt_1/CuO and Pt_1@CuO catalysts, which also shifts to a higher energy region. This observation illustrates that the Pt_1 CuO catalyst with unified Pt O Cu moieties gives a higher proportion of

positively charged Pt atoms, likely through electron back donation from Pt to Cu induced by EMSIs.[22]

As the Cu 3*p* doublet-peaks overlap with the Pt 4*f* curves, Pt $4d_{5/2}$ X-ray photoelectron spectroscopy (XPS) spectra were employed to determine the electronic states of Pt species in these single-atom catalysts.[23] As shown in Figure 2e and Figure S10, the peak centered at 312.3 eV is ascribed to the Pt Cu component, which can only be found in the spectrum of the Pt_1/CuO sample.[23b] Peaks at binding energies of 314.4 and 317.5 eV are indicative of the metallic Pt^0 and positively charged $Pt^{\delta+}$ species, respectively.[15,23b] Notably, the proportion of metallic Pt^0 species decreases from 67.3% in the Pt_1/CuO sample to 7.5% in the Pt_1 CuO catalyst (Table S5). This phenomenon suggests that the Pt atoms donate more electrons to CuO supports through enhanced EMSI in the Pt_1 CuO catalyst. The Cu 2*p* and Cu LMM spectra were subsequently investigated to establish how these EMSIs influence the valence state of Cu. The Cu $2p_{3/2}$ and $2p_{1/2}$ spectra can be fitted into two characteristic peaks (Figure 2f, Figure S11).[24] Peaks centered at 932.1 and 952.0 eV are assigned to the Cu^+ species, whereas Cu^{2+} species are indicated by dominant peaks centered at 933.6 and 953.7 eV.[25] The proportion of Cu^+ /(Cu^+ + Cu^{2+}) in each catalyst was subsequently evaluated quantitatively, using the associated Cu LMM spectra (Figure 2g; Fig-ure S12).[25b] Accordingly, the ratio of evaluated Cu^+ species decreases from 19.4%, 13.5%, and 10.4%, for the Pt_1 CuO, Pt_1@CuO, and Pt_1/CuO catalysts, respectively. The higher proportion of Cu^+ species present in the Pt_1 CuO sample is, again, ascribed to the strengthened electron back donation from Pt sites, in accordance with the changes of the Pt valence state.

Further evidence for the presence of Cu^+ species in the Pt_1 CuO catalyst was acquired by X-ray diffraction (XRD; Figure S13). The signals of Cu_2O diffraction at 2θ = 36.3° and 42.2° can only be found in the Pt_1 CuO sample, which is less prominent in other patterns. Collectively, the aforemen-tioned results demonstrate that the atomic Pt sites with diverse coordination bonds exhibit different interactions with the CuO supports. The Pt_1 CuO catalyst, produced from the calcination of a Pt_1 $Cu(OH)_x$ precursor, exhibits the strongest EMSIs. Such interactions promote the charge redistribution by facilitating the electron donation from Pt to CuO in great propensity. The resulting positively charged Pt sites are highly efficient in activating organic molecules. Meanwhile, the induced charge transfer can also weaken adjacent Cu O bonds (see temperature-programmed reduc-tion experiments in Figure S14), which in-turn facilitates the activation of lattice oxygen atoms to participate in the oxidation processes, leading to the regeneration of oxygen vacancies (Figures S15 and S16).[26]

Catalytic Performance Evaluation

To determine the influence of EMSIs on the catalytic performance of SACs, all synthesized materials were subsequently employed for acetone oxidation (Figure 3; Table S1). As expected, the bare CuO support exhibits a comparatively poor activity where none of the acetone can be oxidized even at 190 °C. This observation suggests that the supported Pt species are active sites for acetone oxidation at low temperatures. The catalytic performance of these materials correlates with the bonding methods be-tween Pt atoms and CuO supports (Figure 3a). The highest

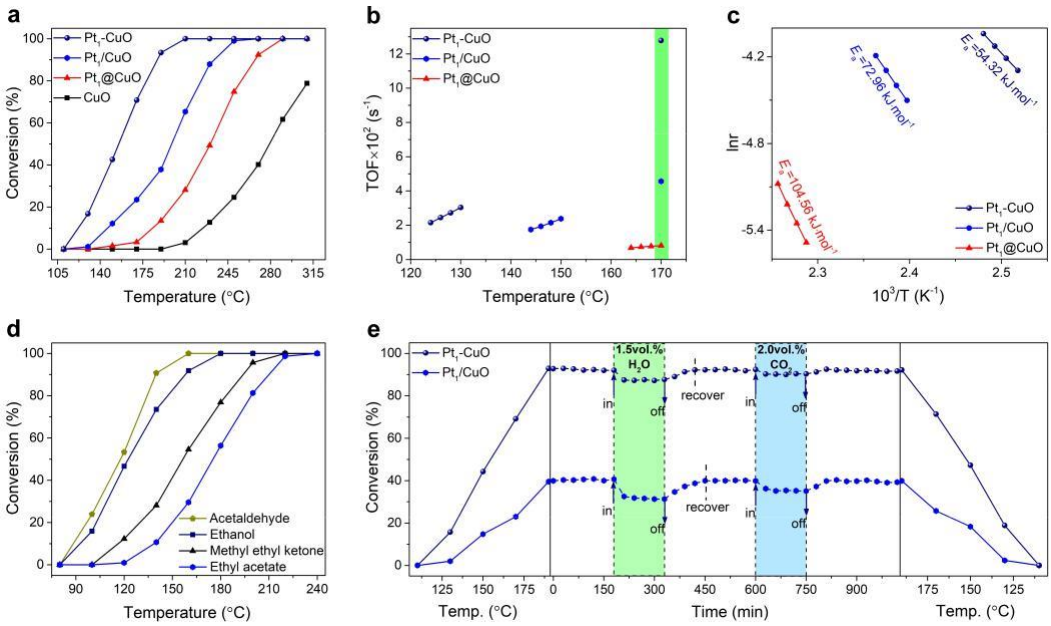

Figure 3. The evaluated a) activity, b) turnover frequency, and c) Arrhenius plots of synthesized catalysts in acetone catalytic oxidation. d) The light-off curves of the Pt_1 CuO catalyst for the oxidation of typical industrial organic pollutants. e) Stability test of the Pt_1 CuO and Pt_1/CuO catalysts for acetone oxidation under different reaction atmospheres.

efficiency is observed over the Pt_1 CuO catalyst, where 800 ppm of acetone can be fully oxidized at just 210 °C (GHSV of 42000 h^{-1}). The associated initiation temperature is below 120 °C. In contrast, the Pt_1/CuO and Pt_1@CuO catalysts are inactive for acetone oxidation at 120 °C, where 90% of acetone can be decomposed at 234 and 267 °C, respectively. Subsequently, the monitored CO_2 selectivity for each catalyst further demonstrated that the Pt_1 CuO catalyst, possessing the strongest EMSIs, is the most efficient active site for the deep, low-temperature oxidation of acetone (Figure S17).

This trend in activity was further evidenced through consideration of the associated turnover frequencies (TOFs; Figure 3b). The Pt_1 CuO catalyst exhibits the highest TOF (0.13 s^{-1}) at 170 °C, which is 2.6 and 16.3 times higher than that of the Pt_1/CuO (0.05 s^{-1}) and Pt_1@CuO (0.008 s^{-1}) catalysts, respectively. Accordingly, the Arrhenius plots were established to determine the activation energy by utilizing the aforementioned data (Figure 3c). The activation energy of the Pt_1/CuO (54.32 kJmol $^{-1}$) catalyst is substan-tially lower than that determined over the Pt_1/CuO (72.96 kJmol $^{-1}$) and Pt_1@CuO (104.56 kJmol $^{-1}$) samples during acetone oxidation. Notably, the synthesized Pt_1 CuO SAC also exhibits superb performance compared to that of the Pt_{NPs}/CuO and Pt_{clu}/CuO catalysts for acetone oxidation (Figure S18). These results further evidence that the strong EMSIs through the unified Pt O Cu moieties significantly promote the catalytic performance of Pt_1 CuO SAC in oxidizing acetone. Additionally, when decreasing the Pt loading content, the single-atom Pt_1 CuO, Pt_1/CuO, and Pt_1@CuO catalysts with a lower loading content of 0.2 wt% were synthesized. As illustrated in Figure S19a, the sup-ported Pt species are atomically dispersed on all these catalyst surfaces, and no clusters or nanoparticles can be detected. When tested for acetone oxidation, the 0.19 wt% Pt_1 CuO catalyst exhibits better performance than that of 0.20 wt% Pt_1/CuO and 0.19 wt% Pt_1@CuO catalysts (Fig-ure S19b,c).

Importantly, to establish whether this was a universal effect, a series of other OVOCs were used as substrates (Figure 3d). For each of these additional substrates, the currently reported catalysts were also displayed for compar-ison, as summarized in Tables S6–S9. The Pt_1 CuO catalyst is evidently highly active for the catalytic oxidation of typical industrial OVOCs, including acetaldehyde (T_{90} at 140 °C), ethanol (T_{90} at 158 °C), methyl ethyl ketone (T_{90} at 195 °C), and ethyl acetate (T_{90} at 211 °C). These results indicate that the Pt_1 CuO SAC with strong EMSIs, is a promising and universal catalyst for the oxidation of OVOCs.

The stability of SACs is usually an important area of concern when employed in thermal reactions. To assess how these different EMSIs influence the stability of prepared Pt_1 CuO and Pt_1/CuO SACs, the H_2O and CO_2 resistances of these catalysts were examined between a heating and cooling cycle (Figure 3e). For both catalysts, water vapor and CO_2 were determined to have a negative impact on catalytic performance, which is likely ascribed to the competitive adsorption between these impurities and reac-tants. Drops in acetone conversion of ca. 5.2% and 8.5% were observed over the Pt_1 CuO and Pt_1/CuO catalysts, respectively, when 1.5 vol.% water vapor was introduced into the stream. Interestingly, after the water vapor was removed from the stream, the original activity was restored for both catalysts within 90 and 120 min, respectively. A similar observation was also made when a 2.0 vol.% CO_2 mixture was added to the reaction stream. The morphology and Pt species of the spent Pt_1 CuO catalyst after the stability test were investigated. As displayed in Figure S20a, the catalyst maintains its regular nanorod morphology. Additionally, the supported Pt sites are atomically dispersed on the support and no aggregation phenomenon can be observed (Figure S20b–e). The above stability test results imply that the strong EMSIs significantly promote the stability of the Pt_1 CuO catalyst in acetone oxidation by restraining the competitive adsorption of reactants and other impurities. The enhanced adsorption and activation of active oxygen species by the Cu_2O CuO interface formed through the EMSIs (Figure S13) is considered as another reason for the better performance of the Pt_1 CuO catalyst in acetone oxidation.[24b] Moreover, the better stability of the Pt_1 CuO sample can also be ascribed to its abundant surface acid sites and hydroxyl species (Figures S21 and S22).

Surface Mechanism of Acetone Oxidation

To understand how these EMSIs influence the surface mechanism, further experiments were required. First, numerous in situ DRIFTS (diffuse reflectance infrared spectroscopy) were recorded (Figure 4; Figures S23 and S24).

The sharp adsorption bands observed at 1695–1698 cm^{-1} are assigned to gaseous acetone, which gradually decreased as the temperature increased (Figure 4a,b).[27] An additional

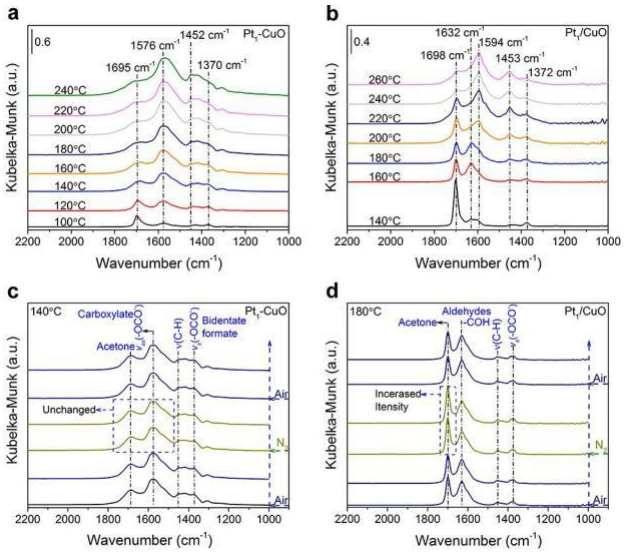

Figure 4. In situ DRIFTS of acetone oxidation as a function of temperature from 100 to 260 °C over a) Pt_1 CuO and b) Pt_1/CuO catalysts. In situ DRIFTS of acetone oxidation under various reaction conditions at c) 140 °C over Pt_1 CuO catalyst and d) 180 °C over Pt_1/CuO catalyst.

broad adsorption band around 1576–1594 cm ^{1} can be ascribed to the asymmetric stretching vibration of a ν_{as}-(OCO) species, where its intensity has a positive relation-ship with the temperature.[28] This band is likely attributed to the carboxylate species resulting from the cleavage of the C C bonds, followed by combination with the active oxygen species.[27] Correspondingly, adsorption bands at 1370– 1372 cm ^{1} were observed, which correspond to the bridging monodentate symmetrical ν_S(OCO) mode from the biden-tate format species, produced by activating the C=O bonds over the Pt sites.[29] Furthermore, the C H bond stretching of the surface-adsorbed methyl/methylene (CH_3/ CH_2) species dominates the spectra between 1452–1453 cm ^{1}.[30] Interestingly, an adsorption band at ca. 1632 cm ^{1}, indicative of the COH bond from the surface-adsorbed aldehyde species, was only observed over the Pt_1/CuO sample at a relatively low temperature (from 140 to 200 °C; Figure 4b).[30] This bond will disappear when the temperature reaches 200 °C, and no such band can be observed over the Pt_1 CuO catalyst. This observation suggests that the aldehyde species is a primary intermediate when reactions are conducted over the Pt_1/CuO catalyst. It is hypothesized that the uncoordi-nated carbonyl species bond with the dissociated H atoms from the CH_3 groups when there are insufficient active oxygen species present.

To further probe the occurrence of surface mechanisms, sequential in situ DRIFTS was conducted at T_{20} (the temperature at which 20% of acetone is converted), where the reaction atmosphere was switched between air and N_2. Notably, for the Pt_1 CuO catalyst (Figure 4c), the peaks indicative of the surface-adsorbed acetone and carbonate species remained unchanged when the air was replaced with N_2. This suggests that the process of acetone oxidation over the Pt_1 CuO catalyst proceeds via a Mars–van Krevelen (MvK) mechanism, where the lattice oxygen atoms are determined as the active oxygen species due to the weakening of O Cu bonds induced by the strong EMSIs.[26] Notably, the absorption band of acetone molecules is significantly strengthened over the Pt_1/CuO catalyst after introducing a N_2 atmosphere, which is restored to the original value while the air was refilled to the cavity (Figure 4d). This phenomenon reveals that the acetone oxidation over the Pt_1/CuO catalyst is strongly influenced by the presence of adsorbed oxygen species. Therefore, it predominantly proceeds via the Langmuir–Hinshelwood (L– H) mechanism.[2a] Given that some of the surface intermedi-ates are observed, the EMSIs do indeed appear to influence the surface mechanisms that take place in this reaction.

Intrinsic Mechanism Determination

We propose that the EMSI modulation of a Pt_1 CuO SAC dramatically promotes its catalytic efficiency for acetone oxidation. The strong EMSIs, which are derived from the polarization of the Pt O Cu moieties, facilitate charge redistribution through electron transfer from Pt atoms to CuO supports. To further explore this hypothesis, a more detailed understanding of the structure–activity relationship in these catalysts was required. Primarily, the adsorption and activation of acetone, considered to be the rate-determining step in this oxidation reaction, was studied by in situ DRIFTS and operando near-ambient pressure XPS (NAP-XPS). The acetone adsorption process was monitored by in situ DRIFTS as a function of adsorption equilibrium times (Figure 5a,b; Figure S25). From 1 to 15 min after introducing 800 ppm acetone, the Pt_1 CuO catalyst exhib-ited the most intense adsorption peak at 1695–1698 cm ^{1} among these three samples, indicating that it possesses the strongest capacity for acetone adsorption. This property is ascribed to the higher proportion of atomic $Pt^{\delta+}$ species induced by the strong EMSIs in the Pt_1 CuO catalyst (Figure 2e). The electronegativity of carbonyl species in acetone molecules allows easy adsorption on the positively charged Pt atoms (via the C=O bond).

To specifically reveal the active sites for acetone activation, operando NAP-XPS was used to probe the Pt 4$d_{5/2}$ region of the representative catalysts during acetone oxidation. As determined from previous analyses, the characteristic peaks around 314.4 and 317.5 eV are indica-tive of the Pt^0 and $Pt^{\delta+}$ species, respectively.[15,23b] For the Pt_1 CuO catalyst (Figure 5c), the ratio of metallic Pt species gradually increases from 7.5% (fresh sample at RT) to 66.5% (180 °C with 200 ppm acetone) during investigations. The increased proportion of Pt^0 species is correlated with the electron transfer from carbonyl groups to positively charged Pt atoms, which we have established occurs during the acetone adsorption and activation processes. Interest-ingly, the ratio of Pt^0 species is partly replenished (to 21.1%) after re-exposure to air atmosphere at room temper-ature. These observations demonstrate that the positively charged Pt atoms in the Pt_1 CuO catalyst are superior sites for activating acetone molecules. On the contrary, the opposite situation is observed over the Pt_1/CuO catalyst

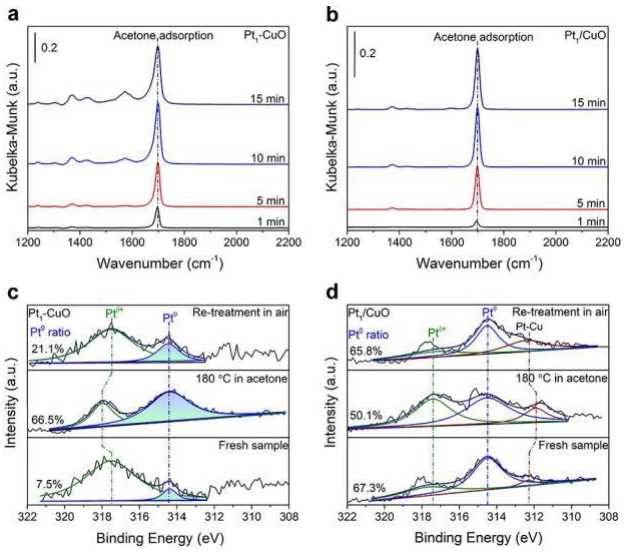

Figure 5. In situ DRIFTS of acetone adsorption as a function of time at room temperature over a) Pt_1 CuO and b) Pt_1/CuO catalysts. Oper-ando Pt 4$d_{5/2}$ NAP-XPS spectra of c) Pt_1 CuO and d) Pt_1/CuO catalysts obtained from the acetone oxidation process.

(Figure 5d). During this analogous experiment, the decline of Pt^0 content (from 67.3% to 50.1%) is attributed to the bonding of Pt sites with the O atoms in the reaction, which implies that the metallic Pt sites in the Pt_1/CuO catalyst are inclined to activate the surface-adsorbed oxygen atoms instead of acetone molecules.

Subsequently, ^{18}O isotopic labeling experiments were conducted to monitor how the oxygen species were activated and consumed during the reaction.[15] As analyzed for the Pt_1 CuO catalyst (Figure 6a), a signal indicative of the $C^{16}O_2$ species is detected as the temperature reached 111 °C, significantly lower than that of the $C^{16}O^{18}O$ (123 °C) and $C^{18}O_2$ (183 °C) species. Furthermore, the signature associ-ated with the $C^{16}O_2$ species reached a maximum value at ca. 239 °C and followed by a drop-off, which was attributed to the exhaustion of available lattice oxygen species. These results emphasize that the lattice oxygen atoms are critical for acetone oxidation over the Pt_1 CuO catalyst. The activation of lattice oxygen atoms is ascribed to the stretch of Cu O bonds induced by strong EMSIs, resulting in reserved oxygen vacancies, which will be refilled by the surface oxygen atoms from the reaction atmosphere. In comparison, when the Pt_1/CuO catalyst was monitored, (Figure 6b) no $C^{16}O_2$ signal was observed during this investigation. Instead, only signals indicative of $C^{16}O^{18}O$ and $C^{18}O_2$ species were observed, initiating at 183 °C and 140 °C, respectively. The observations indicate that the surface-adsorbed oxygen atoms are responsible for producing the active oxygen species to oxidize acetone molecules over the Pt_1/CuO catalyst.

The activation and transformation of oxygen species over each type of SAC were further evaluated using O 1s NAP-XPS spectra (Figure 6c,d). The peaks centered at ca. 529.5–529.3 eV are indicative of the lattice oxygen (O_{latt}) species, while the peaks observed at the binding energies of 530.9–531.5 and 532.5–533.1 eV are assigned to the surface adsorbed oxygen (O_{ads}) and adsorbed H_2O groups, respectively.[31] The changes of O 1s curves over the Pt_1/CuO catalyst were recorded, simulating the conditions employed in the performance evaluation (Figure 6d). Notably, the ratio of O_{ads} species gradually decreased from 49.6% (fresh sample) to 17.9% after exposure to the reactants at 180 °C, which was almost replenished (34.9%) by exposure to air at room temperature. This observation further confirms that the active oxygen species formed over the Pt_1/CuO catalyst during acetone oxidation are primarily derived from the surface-adsorbed oxygen atoms. In comparison, for the Pt_1 CuO catalyst (Figure 6c) the O 1s NAP-XPS spectra reveal that the O_{latt} species are consumed in the reaction, which decrease from 71.1% (fresh sample) to 59.1% (120 °C) and 54.6% (180 °C), and then increased to 66.4% after re-exposure to air at room temperature. This phenom-enon underlines our above analyses that the strong EMSI in the Pt_1 CuO catalyst will weaken the Cu O bonds and, in-turn, facilitate the activation of lattice oxygen atoms to participate in the oxidation reaction.[26]

The electronic structure and adsorption energy were subsequently illustrated by DFT studies. From the charge density difference analysis (Figure 7a–c; Figure S26), the yellow and blue areas represent the increase and decrease of charge density, respectively. The cutoff of density-difference iso-surface is equal to 0.01 electronsÅ ^{3}. Distinctly, more intense electron transfer between Pt atoms and CuO supports was observed over the Pt_1 CuO catalyst compared with Pt_1/CuO and Pt_1@CuO catalysts, resulting in abundant positively charged Pt species, in accordance with our experimental results. The energy of acetone and O_2 adsorption over these SACs was further evaluated (Fig-ure S27). The energy of acetone adsorption over these atomic $Pt^{\delta+}$ sites was determined to be 0.98 eV, which is much lower than that of O_2 adsorption (0.64 eV), indicat-ing that these positively charged Pt atoms in the Pt_1 CuO catalyst exist prior to adsorption and activation of acetone molecules. Comparatively, the metallic Pt sites exhibited the higher capacity to adsorb surface oxygen species with an

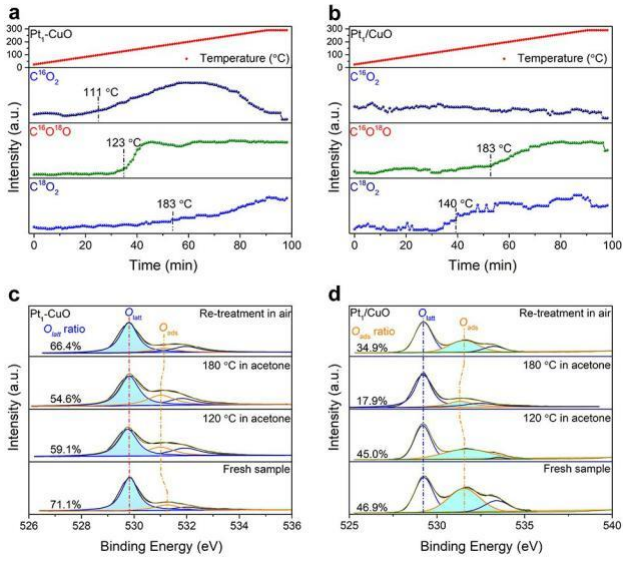

Figure 6. ^{18}O isotopic labeling experiment in the temperature-programmed oxidation of acetone over a) Pt_1 CuO and b) Pt_1/CuO catalysts. Operando O 1s NAP-XPS spectra of c) Pt_1 CuO and d) Pt_1/CuO catalysts obtained from the acetone oxidation process.

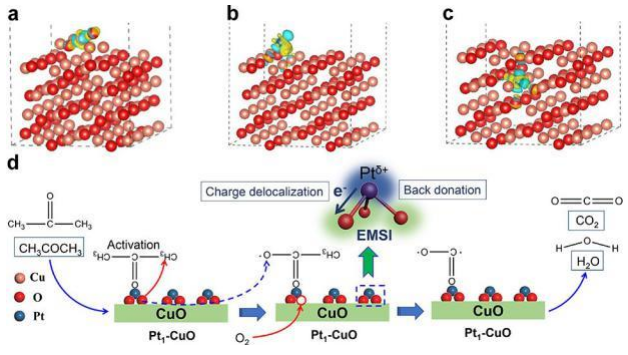

Figure 7. Calculated charge density differences (side view) of a) Pt_1 CuO, b) Pt_1/CuO, and c) Pt_1@CuO catalysts. d) Proposed intrinsic mechanism of acetone oxidation over the EMSI-modulated Pt_1 CuO catalyst.

adsorption energy of 1.90 eV over the Pt_1/CuO sample, which is further confirmed by the O_2 TPD (temperature-programmed desorption) results (Figure S28).

Finally, the intrinsic mechanism of acetone oxidation over the EMSI-modulated Pt_1 CuO catalyst is revealed in an atomic scale (Figure 7d). The strong electronic interactions between Pt atoms and CuO supports through the unified Pt O Cu coordination bonds facilitate charge transfer from Pt to Cu, thereby producing abundant positively charged Pt species. The acetone molecules are adsorbed and activated over these atomic $Pt^{\delta+}$ sites. Subsequently, the vicinal C C bonds are cleaved, a process which is promoted by the electron deficient carbonyl groups, leading to the formation of CH_3CO* species. Meanwhile, the lattice oxy-gen atoms around the Pt atoms are activated to dissociate O* species, which will combine with CH_3CO* to form CH_3COO* species. Subsequently, the *COO* intermediates are produced through α-H abstraction and C C cleavage. This formate species is totally decomposed into harmless CO_2 and H_2O products over the catalyst surface. Accord-ingly, the strong EMSIs between the Pt atoms and CuO supports are decisive for this reaction. The EMSIs consist of charge redistribution through the unified Pt O Cu coordi-nation bonds, which modulate the *d*-band structure of the Pt atoms and strengthens the adsorption and activation of reactants. Hence, the energy barrier is lowered, and the rate-limiting step is facilitated.

Conclusion

In summary, three analogous catalysts with different EMSIs were carefully designed and synthesized. A positive correla-tion between the strength of the EMSIs and catalyst performance was observed. Surprisingly, the Pt_1 CuO SAC with the unified bonding exhibited the strongest EMSI, which can fully convert 800 ppm of acetone into CO_2 at just 210 °C with a low activation energy of 54.32 kJmol ^{1}. On the basis of operando methods and DFT studies, the EMSIs promote electron back donation from Pt to CuO, producing sufficiently positively charged Pt atoms, which are highly efficient sites in activating acetone at low temperatures. Meanwhile, the charge redistribution through the unified Pt O Cu bonds will facilitate the activation of adjacent lattice oxygens to participate in oxidation, leading to the circulation of oxygen vacancies. Ultimately, what this study demonstrates is that dramatic increments in catalyst performance can be acquired simply by promoting EMSIs in SACs. Herein, we have shown this to be true for Pt_1 CuO and demonstrated that these enhancements are not limited to a specific substrate. We therefore conclude that such EMSIs must be considered when studying SACs, as their influence on the catalysis is significant.

Acknowledgements

This work was financially supported by the National Natural Science Foundation of China (21922606, 21876139), the Key R&D Program of Shaanxi Province (2019SF-244, 2019ZDLSF05-05-02), and the Shaanxi Natural Science Fundamental Shaanxi Coal Chemical Joint Fund (2019JLM-14). The authors gratefully acknowledge support from the K. C. Wong Education Foundation and Institute of High Energy Physics (CAS) for XANES and EXAFS analyses.

Conflict of Interest

The authors declare no conflict of interest.

Data Availability Statement

The data that support the findings of this study are available in the Supporting Information of this article.

Keywords: Acetone Oxidation · Electronic Metal-Support Interactions · Intrinsic Mechanism · Single-Atom Catalysts

[1] a) J.-H. Park, A. H. Goldstein, J. Timkovsky, S. Fares, R. Weber, J. Karlik, R. Holzinger, *Science* **2013**, *341*, 643–647; b) P. Wang, Y. Chen, J. Hu, H. Zhang, Q. Ying, *Environ. Sci. Technol.* **2019**, *53*, 1404–1412; *c)* Q. He, S. Tomaz, C. Li, M. Zhu, D. Meidan, M. Riva, A. Laskin, S. S. Brown, C. George, X. Wang, Y. Rudich, *Environ. Sci. Technol.* **2021**, *55*, 2878–2889.

[2] a) Z. Jiang, C. He, N. F. Dummer, J. Shi, M. Tian, C. Ma, Z. Hao, S. H. Taylor, M. Ma, Z. Shen, *Appl. Catal. B* **2018**, *226*, 220–233; b) C. He, Z. Jiang, M. Ma, X. Zhang, M. Douthwaite, J.-W. Shi, Z. Hao, *ACS Catal.* **2018**, *8*, 4213–4229; c) M. Huang, Y. Li, M. Li, J. Zhao, Y. Zhu, C. Wang, V. K. Sharma, *Environ. Sci. Technol.* **2019**, *53*, 3610–3619.

[3] Y. Zheng, Q. Liu, C. Shan, Y. Su, K. Fu, S. Lu, R. Han, C. Song, N. Ji, D. Ma, *Environ. Sci. Technol.* **2021**, *55*, 5403–5411.

[4] P. Wu, X. Jin, Y. Qiu, D. Ye, *Environ. Sci. Technol.* **2021**, *55*, 4268–4286.

[5] C. He, J. Cheng, X. Zhang, M. Douthwaite, S. Pattisson, Z. Hao, *Chem. Rev.* **2019**, *119*, 4471–4568.

[6] Q. Wang, Y. Li, A. Serrano-Lotina, W. Han, R. Portela, R. Wang, M. A. Banares, K. L. Yeung, *J. Am. Chem. Soc.* **2021**, *143*, 196–205.

[7] a) Y. Chen, J. Gao, Z. Huang, M. Zhou, J. Chen, C. Li, Z. Ma, J. Chen, X. Tang, *Environ. Sci. Technol.* **2017**, *51*, 7084–7090; b) T. Gan, J. Yang, D. Morris, X. Chu, P. Zhang, W. Zhang, Y. Zou, W. Yan, S. H. Wei, G. Liu, *Nat. Commun.* **2021**, *12*, 2741; c) P. Hu, Z. Huang, Z. Amghouz, M. Makkee, F. Xu, F. Kapteijn, A. Dikhtiarenko, Y. Chen, X. Gu, X. Tang, *Angew. Chem. Int. Ed.* **2014**, *53*, 3418–3421; *Angew. Chem.* **2014**, *126*, 3486–3489.

[8] Z. Jiang, X. Feng, J. Deng, C. He, M. Douthwaite, Y. Yu, J. Liu, Z. Hao, Z. Zhao, *Adv. Funct. Mater.* **2019**, *29*, 1902041.

[9] a) R. Lang, X. Du, Y. Huang, X. Jiang, Q. Zhang, Y. Guo, K. Liu, B. Qiao, A. Wang, T. Zhang, *Chem. Rev.* **2020**, *120*, 11986–12043; b) Y. Zhu, S. F. Yuk, J. Zheng, M.-T. Nguyen, M.-S. Lee, J. Szanyi, L. Kovarik, Z. Zhu, M. Balasubramanian, V.-A. Glezakou, J. L. Fulton, J. A. Lercher, R. Rousseau, O. Y. Gutiérrez, *J. Am. Chem. Soc.* **2021**, *143*, 5540–5549; c) W. Qu, X. Liu, J. Chen, Y. Dong, X. Tang, Y. Chen, *Nat. Commun.* **2020**, *11*, 1532.

[10] a) C. T. Campbell, *Nat. Chem.* **2012**, *4*, 597–598; b) A. Bruix, J. A. Rodriguez, P. J. Ramirez, S. D. Senanayake, J. Evans,

J. B. Park, D. Stacchiola, P. Liu, J. Hrbek, F. Illas, *J. Am. Chem. Soc.* **2012**, *134*, 8968–8974.

[11] a) L. Liu, A. Corma, *Chem. Rev.* **2018**, *118*, 4981–5079; b) V. Muravev, G. Spezzati, Y.-Q. Su, A. Parastaev, F.-K. Chiang, A. Longo, C. Escudero, N. Kosinov, E. J. M. Hensen, *Nat. Catal.* **2021**, *4*, 469–478; **c)** Y. Shi, Z.-R. Ma, Y.-Y. Xiao, Y.-C. Yin, W.-M. Huang, Z.-C. Huang, Y.-Z. Zheng, F.-Y. Mu, R. Huang, G.-Y. Shi, Y.-Y. Sun, X.-H. Xia, W. Chen, *Nat. Commun.* **2021**, *12*, 3021; d) J. Liu, Q. Guan, H. Wu, W. Liu, Y. Lin, Z. Sun, X. Ye, X. Zheng, H. Pan, J. Zhu, S. Chen, W. Zhang, S. Wei, J. Lu, *J. Am. Chem. Soc.* **2019**, *141*, 14515–14519; e) L. Wang, C. Zhu, M. Xu, C. Zhao, J. Gu, L. Cao, X. Zhang, Z. Sun, S. Wei, W. Zhou, W.-X. Li, J. Lu, *J. Am. Chem. Soc.* **2021**, *143*, 18854–18858.

[12] X. I. Pereira-Hernandez, A. DeLaRiva, V. Muravev, D. Kunwar, H. Xiong, B. Sudduth, M. Engelhard, L. Kovarik, E. J. M. Hensen, Y. Wang, A. K. Datye, *Nat. Commun.* **2019**, *10*, 1358.

[13] Z. Jiang, M. Jing, X. Feng, J. Xiong, C. He, M. Douthwaite, L. Zheng, W. Song, J. Liu, Z. Qu, *Appl. Catal. B* **2020**, *278*, 119304.

[14] a) X. Song, L. Huang, W. He, C. Liu, F. Hu, Y. Jiang, Z. Sun, S. Wei, *J. Phys. Chem. C* **2019**, *123*, 10907–10916; b) C. Zhang, L. Chao, L. Wang, Y. Cheng, Q. Xie, *Electrochim. Acta* **2020**, *330*, 135234; *c)* G. Chen, Y. Zhao, G. Fu, P. N. Duchesne, L. Gu, Y. Zheng, X. Weng, M. Chen, P. Zhang, C. W. Pao, J. F. Lee, N. Zheng, *Science* **2014**, *344*, 495–499.

[15] A. J. Therrien, A. J. R. Hensley, M. D. Marcinkowski, R. Zhang, F. R. Lucci, B. Coughlin, A. C. Schilling, J.-S. McEwen, E. C. H. Sykes, *Nat. Catal.* **2018**, *1*, 192–198.

[16] D. Yang, Q. Zhu, C. Chen, H. Liu, Z. Liu, Z. Zhao, X. Zhang, S. Liu, B. Han, *Nat. Commun.* **2019**, *10*, 677.

[17] N. Cheng, S. Stambula, D. Wang, M. N. Banis, J. Liu, A. Riese, B. Xiao, R. Li, T. K. Sham, L. M. Liu, G. A. Botton, X. Sun, *Nat. Commun.* **2016**, *7*, 13638.

[18] a) H. V. Thang, G. Pacchioni, L. DeRita, P. Christopher, *J. Catal.* **2018**, *367*, 104–114; *b)* H. A. Aleksandrov, K. M. Neyman, K. I. Hadjiivanovd, G. N. Vayssilov, *Phys. Chem. Chem. Phys.* **2016**, *18*, 22108–22121.

[19] L. Nie, D. Mei, H. Xiong, B. Peng, Z. Ren, X. I. P. Hernandez, A. DeLaRiva, M. Wang, M. H. Engelhard, L. Kovarik, A. K. Datye, Y. Wang, *Science* **2017**, *358*, 1419–1423.

[20] a) L. DeRita, S. Dai, K. Lopez-Zepeda, N. Pham, G. W. Graham, X. Pan, P. Christopher, *J. Am. Chem. Soc.* **2017**, *139*, 14150–14165; b) G. Sun, Z.-J. Zhao, R. Mu, S. Zha, L. Li, S. Chen, K. Zang, J. Luo, Z. Li, S. C. Purdy, A. J. Kropf, J. T. Miller, L. Zeng, J. Gong, *Nat. Commun.* **2018**, *9*, 4454; c) Q. Liu, Z. Zhang, *Catal. Sci. Technol.* **2019**, *9*, 4821–4834.

[21] Y. Qu, B. Chen, Z. Li, X. Duan, L. Wang, Y. Lin, T. Yuan, F. Zhou, Y. Hu, Z. Yang, C. Zhao, J. Wang, C. Zhao, Y. Hu, G. Wu, Q. Zhang, Q. Xu, B. Liu, P. Gao, R. You, W. Huang, L. Zheng, L. Gu, Y. Wu, Y. Li, *J. Am. Chem. Soc.* **2019**, *141*, 4505–4509.

[22] M. Moliner, J. E. Gabay, C. E. Kliewer, R. T. Carr, J. Guzman, G. L. Casty, P. Serna, A. Corma, *J. Am. Chem. Soc.* **2016**, *138*, 15743–15750.

[23] a) I. Khalakhan, M. Vorokhta, X. Xie, L. Piliai, I. Matolínová, *J. Electron Spectrosc.* **2021**, *246*, 147027; *b)* L. E. Gómez, B. M. Sollier, M. D. Mizrahi, J. M. Ramallo López, E. E. Miró, A. V. Biox, *Int. J. Hydrogen Energy* **2014**, *39*, 3719–3729.

[24] a) T.-T. Zhuang, Y. Pang, Z.-Q. Liang, Z. Wang, Y. Li, C.-S. Tan, J. Li, C. T. Dinh, P. De Luna, P.-L. Hsieh, T. Burdyny, H.-H. Li, M. Liu, Y. Wang, F. Li, A. Proppe, A. Johnston, D.-H. Nam, Z.-Y. Wu, Y.-R. Zheng, A. H. Ip, H. Tan, L.-J. Chen, S.-H. Yu, S. O. Kelley, D. Sinton, E. H. Sargent, *Nat. Catal.* **2018**, *1*, 946–951; **b)** Y. Shi, L. Xu, M. Chen, B. Yang, G. Cheng, C.-E. Wu, Z. Miao, N. Wang, X. Hu, *J. Ind. Eng. Chem.* **2022**, *105*, 324–336.

[25] a) N. J. Divins, D. Kordus, J. Timoshenko, I. Sinev, I. Zegkinoglou, A. Bergmann, S. W. Chee, S. Widrinna, O. Karslioglu, H. Mistry, M. Lopez Luna, J. Q. Zhong, A. S. Hoffman, A. Boubnov, J. A. Boscoboinik, M. Heggen, R. E. Dunin-Borkowski, S. R. Bare, B. R. Cuenya, *Nat. Commun.* **2021**, *12*, 1435; b) Z. Q. Liang, T. T. Zhuang, A. Seifitokaldani, J. Li, C. W. Huang, C. S. Tan, Y. Li, P. De Luna, C. T. Dinh, Y. Hu, Q. Xiao, P. L. Hsieh, Y. Wang, F. Li, R. Quintero-Bermudez, Y. Zhou, P. Chen, Y. Pang, S. C. Lo, L. J. Chen, H. Tan, Z. Xu, S. Zhao, D. Sinton, E. H. Sargent, *Nat. Commun.* **2018**, *9*, 3828; c) D. Wakerley, S. Lamaison, F. Ozanam, N. Menguy, D. Mercier, P. Marcus, M. Fontecave, V. Mougel, *Nat. Mater.* **2019**, *18*, 1222–1227.

[26] X. Liu, S. Jia, M. Yang, Y. Tang, Y. Wen, S. Chu, J. Wang, B. Shan, R. Chen, *Nat. Commun.* **2020**, *11*, 4240.

[27] Z. Wang, P. Ma, K. Zheng, C. Wang, Y. Liu, H. Dai, C. Wang, H.-C. Hsi, J. Deng, *Appl. Catal. B* **2020**, *274*, 118963.

[28] S. Kattel, B. Yan, Y. Yang, J. G. Chen, P. Liu, *J. Am. Chem. Soc.* **2016**, *138*, 12440–12450.

[29] J. Wang, P. Zhang, J. Li, C. Jiang, R. Yunus, J. Kim, *Environ. Sci. Technol.* **2015**, *49*, 12372–12379.

[30] J. Guo, C. Lin, C. Jiang, P. Zhang, *Appl. Surf. Sci.* **2019**, *475*, 237–255.

[31] a) F. Jiang, S. Wang, B. Liu, J. Liu, L. Wang, Y. Xiao, Y. Xu, X. Liu, *ACS Catal.* **2020**, *10*, 11493–11509; b) H. Pan, Y. Jian, C. Chen, C. He, Z. Hao, Z. Shen, H. Liu, *Environ. Sci. Technol.* **2017**, *51*, 6288–6297; *c)* H. Tan, J. Wang, S. Yu, K. Zhou, *Environ. Sci. Technol.* **2015**, *49*, 8675–8682.